

Towers of Quantum Many-body Scars from Integrable Boundary States

Kazuyuki Sanada,¹ Yuan Miao,² and Hosho Katsura^{1,3,4}

¹*Department of Physics, The University of Tokyo, Hongo, Bunkyo-ku, Tokyo 113-0033, Japan*

²*Kavli Institute for the Physics and Mathematics of the Universe (WPI),*

The University of Tokyo Institutes for Advanced Study,

The University of Tokyo, Kashiwa, Chiba 277-8583, Japan

³*Institute for Physics of Intelligence, The University of Tokyo, Hongo, Bunkyo-ku, Tokyo 113-0033, Japan*

⁴*Trans-scale Quantum Science Institute, The University of Tokyo, Bunkyo-ku, Tokyo 113-0033, Japan*

(Dated: November 5, 2024)

We construct several models with multiple quantum many-body scars (QMBS) using integrable boundary states (IBS). We focus on the tilted Néel states, which are parametrized IBS of the spin-1/2 Heisenberg model, and show that these states can be used to construct a tower of scar states. Our models exhibit periodic revival dynamics, showcasing a characteristic behavior of superpositions of QMBS. Furthermore, the tower of QMBS found in this study possesses a restricted spectrum generating algebra (RSGA) structure, indicating that QMBS are equally spaced in energy. This approach can be extended to two-dimensional models, which can be decomposed into an array of one-dimensional models. In this case, the tilted Néel states again serve as parent states for multiple scar states. These states demonstrate low entanglement entropy, marking them as exact scar states. Notably, their entanglement entropy adheres to the sub-volume law, further solidifying the nonthermal properties of QMBS. Our results provide novel insights into constructing QMBS using IBS, thereby illuminating the connection between QMBS and integrable models.

I. INTRODUCTION

Thermalization in isolated quantum many-body systems is a long-standing puzzle in the study of quantum physics. Initiated by von Neumann's seminal work on quantum ergodic theorem [1], there have been numerous theoretical studies on quantum thermalization [2, 3]. Recently, the eigenstate thermalization hypothesis (ETH) [4–6] has been recognized as a central principle that governs quantum thermalization. ETH provides a framework for explaining the relaxation of quantum many-body systems towards equilibrium. Roughly speaking, the strong version of ETH argues that all energy eigenstates are thermal. It has been demonstrated that the strong ETH holds for many types of quantum systems [7–10]. However, it does not apply to all types of quantum many-body systems; known exceptions include integrable systems [11, 12], many-body localized systems [9, 13–15], and systems with Hilbert space fragmentation [16–18].

Recent advances in experimental technologies, such as quantum simulators with superconducting circuits [19, 20], trapped ions [21], ultracold atoms [22–24], and Rydberg atoms [25, 26], have made it possible to directly observe thermalization processes in quantum systems. This development revealed an exotic class of quantum many-body states that evade thermalization [25]. These nonthermal states are called quantum many-body scars (QMBS), by analogy to quantum scars in single-particle systems [27–29]. Today, it is widely accepted that QMBS refer to energy eigenstates of non-integrable models that violate ETH [30]. To date, a number of systems exhibiting QMBS have been reported in both experimental [31–33] and theoretical studies [16, 30, 34–45]. Some of these systems possess exact QMBS, which can be writ-

ten in closed form. A systematic construction of such models has become a key issue in theoretical studies of QMBS [16, 41, 42, 46–54].

In our previous work [55], we proposed a method for constructing models with QMBS using integrable boundary states (IBS) [56]. These states are associated with a set of conserved charges $\{Q_n\}_{n=2,3,\dots}$ ¹ in quantum integrable models. IBS are defined as states that are annihilated by all parity-odd charges of an integrable Hamiltonian [56–60], i.e., $\{Q_{2k+1}\}_{k=1,2,\dots}$. In other words, an IBS $|\Psi_0\rangle$ is a state for which

$$Q_{2k+1} |\Psi_0\rangle = 0 \quad (1)$$

holds for all $k = 1, 2, \dots$

The IBS play an important role in the study of out-of-equilibrium physics of quantum integrable models [56, 61–63], as well as obtaining correlation functions in the context of AdS/CFT integrability [57, 64–66]. The IBS under consideration are typically quantum states with area-law entanglement entropy scaling, such as product states or matrix product states². One of the remarkable examples is the tilted Néel states for the isotropic and anisotropic Heisenberg spin chains. We will use the tilted Néel states in our paper to construct QMBS.

Our procedure starts with a given IBS $|\Psi_0\rangle$. We identify a nonintegrable operator H_{NI} for which $|\Psi_0\rangle$ is an

¹ The subscript n of the charge Q_n represents the *order* of the charge. It indicates how many consecutive sites its local operator spans.

² There is one notable exception with volume-law entanglement scaling, the crosscap state [67–71], which is out of this article's scope.

eigenstate³. If such a Hamiltonian H_{NI} is found, $|\Psi_0\rangle$ becomes an energy eigenstate of

$$H(\{t_k\}) = H_{\text{NI}} + \sum_{k=1}^{\infty} t_k Q_{2k+1}, \quad (2)$$

where $\{t_k\}_{k=1}^{\infty}$ are real numbers. The state $|\Psi_0\rangle$ can be regarded as an exact QMBS if the Hamiltonian $H(\{t_k\})$ is nonintegrable and the energy of this state lies in the middle of the spectrum. In our previous work [55], we demonstrated the effectiveness of this approach by constructing several families of models with QMBS, e.g., the Majumdar-Ghosh model perturbed by parity-odd charges of the Heisenberg chain. However, the models constructed by this method exhibit only one or two isolated QMBS that do not have any nontrivial dynamics. In this paper, we construct models with multiple QMBS using IBS and show that their dynamics exhibit periodic revivals, which is a typical behavior for a superposition of QMBS [73].

This paper is organized as follows. In Sec. II, we introduce a model with QMBS that are annihilated by the spin-1/2 scalar spin chirality, the third conserved charge of the spin-1/2 XXX model. In Sec. III, we demonstrate that the model introduced in Sec. II can be generalized to the completely anisotropic case, where the scalar spin chirality is replaced with the third conserved charge of the spin-1/2 XYZ model. In other words, the IBS discussed in Sec. II can also serve as parent states of QMBS in the new model. In Sec. IV, we examine the dynamical behavior of a superposition of scar states and compare it with that of a thermal state. In Sec. V, we discuss a higher-dimensional extension of our models constructed in Sec. III. Finally, we conclude and discuss our results in Sec. VI.

II. MODEL WITH U(1) SYMMETRY AND SCARS

We consider a one-dimensional (1D) spin-1/2 model with two- and three-body interactions. The Hamiltonian depends on two parameters g and $h_y \in \mathbb{R}$ and is given by

$$H_1(g, h_y) = C_{\text{SC}} + gH_{\text{pert}} + h_y Y, \quad (3)$$

where

$$C_{\text{SC}} = \sum_{j=1}^L \sigma_j \cdot (\sigma_{j+1} \times \sigma_{j+2}), \quad (4)$$

$$H_{\text{pert}} = \sum_{j=1}^L c_j (\sigma_j^x \sigma_{j+1}^x - \sigma_j^y \sigma_{j+1}^y + \sigma_j^z \sigma_{j+1}^z + 1), \quad (5)$$

$$Y = \sum_{j=1}^L \sigma_j^y. \quad (6)$$

Here σ_j^μ ($\mu = x, y, z$) are the Pauli matrices acting on site j and each of $\{c_j\}_{j=1}^L$ can be any real number. We impose periodic boundary conditions, i.e., $\sigma_{L+1}^\mu = \sigma_1^\mu$, and assume the number of sites L to be even.

The only symmetry of the Hamiltonian H_1 is U(1) symmetry generated by Y , which is the y -component of the total spin. Because of this symmetry, the Hilbert space can be split into different sectors labeled by the eigenvalue of Y . In the following, with a slight abuse of notation, we will denote the eigenvalue of Y by the same symbol.

The Hamiltonian H_1 is unlikely to be integrable since the perturbation term H_{pert} is nonintegrable for randomly chosen $\{c_j\}_{j=1}^L$. To confirm the lack of integrability of the Hamiltonian H_1 , we calculate the distribution $P(s)$ of the energy level spacings in the ascending sorted eigenspectrum $\{E_i\}$, normalized by the mean level spacing Δ , $s_i = (E_i - E_{i-1})/\Delta$. According to the random matrix theory, the level-spacing distribution obeys the Wigner-Dyson distribution

$$P_{\text{WD}}(s) = \frac{32}{\pi^2} s^2 e^{-\frac{4}{\pi} s^2} \quad (7)$$

if the system is nonintegrable⁴ [74, 75], and it obeys the Poisson distribution

$$P_{\text{Poisson}}(s) = e^{-s} \quad (8)$$

if the system is integrable or many-body localized [76]. Figure 1 shows that $P(s)$ of the energy spectrum of H_1 in the sector with $Y = 0$ obeys the GUE Wigner-Dyson distribution rather than the Poisson distribution. It suggests that this Hamiltonian is neither integrable nor in a many-body localized phase.

Having established the non-integrability of the model, we now turn to the construction of QMBS in this model. Our target states are the tilted Néel states parametrized

³ The method in Ref. [72] is particularly useful for finding such an operator.

⁴ More precisely, the level-spacing distribution obeys $P_{\text{WD}}(s)$ when the given system does not have time-reversal symmetry. When the system is nonintegrable and time-reversal invariant, its level spacing distribution obeys the Gaussian β ensemble with $\beta = 1$, i.e., $P(s) = \frac{\pi}{2} s e^{-\frac{\pi}{4} s^2}$.

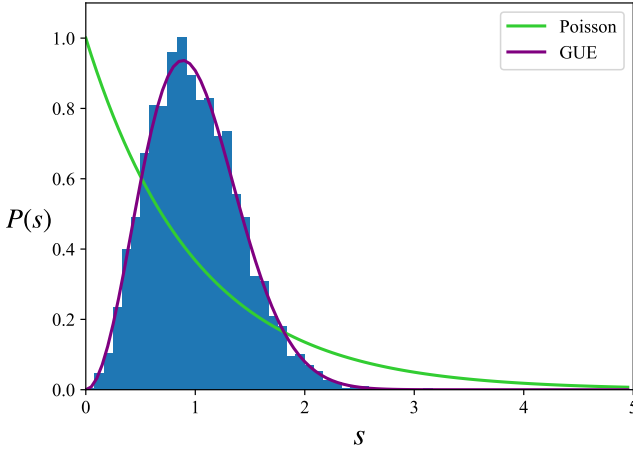


FIG. 1. Level-spacing statistics in the middle half of the spectrum of $H_1(g, h_y)$ [Eq. (3)] with $g = 1$, $h_y = 1$, and $L = 16$. The coefficients c_j are randomly chosen from $[-1, 1]$. The data are taken in the symmetry sector with $Y = 0$. The Wigner-Dyson (GUE) and Poisson distributions are shown for comparison.

by $\alpha \in \mathbb{C}$:

$$|\psi_1(\alpha)\rangle = \frac{1}{\sqrt{\mathcal{N}}} [(-\alpha|\uparrow\rangle + |\downarrow\rangle) \otimes (|\uparrow\rangle + \alpha|\downarrow\rangle)]^{\otimes \frac{L}{2}}, \quad (9)$$

$$|\psi_2(\alpha)\rangle = \frac{1}{\sqrt{\mathcal{N}}} [(|\uparrow\rangle + \alpha|\downarrow\rangle) \otimes (-\alpha|\uparrow\rangle + |\downarrow\rangle)]^{\otimes \frac{L}{2}}, \quad (10)$$

where $|\uparrow\rangle$ and $|\downarrow\rangle$ are normalized eigenstates of σ^z with eigenvalues $+1$ and -1 , respectively. The normalization constant is given by $\mathcal{N} = (|\alpha|^2 + 1)^L$. These states are related to each other by the one-site translation \mathcal{T} .

Since the tilted Néel states $|\psi_{1,2}(\alpha)\rangle$ are IBS of the 1D Heisenberg model [56, 77], they are annihilated by C_{SC} , known as the third conserved charge of the Heisenberg Hamiltonian [78, 79]. On the other hand, H_{pert} is a weighted sum of projection operators onto $\frac{1}{\sqrt{2}}(|\uparrow\uparrow\rangle_{j,j+1} + |\downarrow\downarrow\rangle_{j,j+1})$, each of which annihilates the states $|\psi_{1,2}(\alpha)\rangle$. Since $|\psi_{1,2}(\alpha)\rangle$ are annihilated by C_{SC} and H_{pert} simultaneously, they are zero-energy states of $C_{\text{SC}} + gH_{\text{pert}}$ for all g . We note in passing that the local terms of H_{pert} form a representation of the periodic Temperley–Lieb algebra [80, 81]. This is not surprising, since each local term of H_{pert} is related to the usual isotropic Heisenberg Hamiltonian on two sites by a unitary transformation.

The key to constructing multiple scar states is to note that the parameter α in the tilted Néel states is arbitrary. This allows us to project the tilted Néel states onto states with definite magnetization in the y direction, which remain eigenstates of $H_1(g, h_y)$ with nonzero h_y . To see this, we change the basis from $\{|\uparrow\rangle, |\downarrow\rangle\}$ to the basis in which σ^y is diagonal:

$$|+\rangle = \frac{1}{\sqrt{2}}(|\uparrow\rangle + i|\downarrow\rangle), \quad |-\rangle = \frac{1}{\sqrt{2}}(|\uparrow\rangle - i|\downarrow\rangle). \quad (11)$$

In the new basis, $|\psi_1(\alpha)\rangle$ can be rewritten as

$$\begin{aligned} |\psi_1(\alpha)\rangle &= \left(\frac{\alpha - i}{\sqrt{2}}\right)^L \cdot \frac{i^{L/2}}{\sqrt{\mathcal{N}}} [(z|+\rangle + |-\rangle) \\ &\quad \otimes (z|+\rangle - |-\rangle)]^{\otimes \frac{L}{2}} \\ &= \left(\frac{\alpha - i}{\sqrt{2}}\right)^L \cdot \frac{i^{L/2}}{\sqrt{\mathcal{N}}} \sum_{n=0}^L z^{L-n} \sqrt{\binom{L}{n}} |\Psi_n\rangle, \end{aligned} \quad (12)$$

where $z = \frac{\alpha+i}{\alpha-i}$ and

$$|\Psi_n\rangle = \frac{(\mathcal{O}_\pi^-)^n}{\sqrt{n!L!/(L-n)!}} |+\dots+\rangle \quad (13)$$

with

$$\mathcal{O}_\pi^- = \sum_{j=1}^L (-1)^{j-1} \tilde{\sigma}_j^- = \sum_{j=1}^L \frac{(-1)^{j-1}}{2} (\sigma_j^z - i\sigma_j^x). \quad (14)$$

The states $|\Psi_n\rangle$ are normalized to 1.

Since we can take $z \in \mathbb{C} \setminus \{1\}$ arbitrarily, each $|\Psi_n\rangle$ is an eigenstate of the Hamiltonian (3) with eigenenergy $(L - 2n)h_y$. To confirm that these states are low-entanglement states in the middle of the spectrum, we compute the half-chain entanglement entropies (EE), S_A , of all energy eigenstates. The results are shown in Fig. 2. Clearly, the half-chain EE of $|\Psi_n\rangle$ are significantly lower than those of the other eigenstates, suggesting that these states are exact QMBS. We can analytically compute the half-chain EE of $|\Psi_n\rangle$ following the procedure in our previous work [55] (see also [82]). The result reads

$$S_A(|\Psi_n\rangle) = - \sum_{k=0}^{\min(n, L-n)} \frac{\binom{L/2}{k} \binom{L/2}{n-k}}{\binom{L}{n}} \ln \frac{\binom{L/2}{k} \binom{L/2}{n-k}}{\binom{L}{n}}. \quad (15)$$

For large L at fixed $\frac{n}{L}$, the leading term in $S_A(|\Psi_n\rangle)$ is $\frac{1}{2} \ln L$, which proves that their entanglement entropy obeys a sub-volume law.

We note that the scar states $|\Psi_n\rangle$ cannot be distinguished from the rest of the states by symmetry, as $[C_{\text{SC}}, \mathcal{O}_\pi^-] \neq 0$. However, the presence of a tower of scars can be understood through the restricted spectrum generating algebra (RSGA) [83, 84]. In our system, the Hamiltonian $H_1(g, h_y)$, the reference state $|\Psi_0\rangle$, and the lowering operator \mathcal{O}_π^- satisfy an RSGA of order 2:

$$(i) \quad H_1 |\Psi_0\rangle = Lh_y |\Psi_0\rangle, \quad (16)$$

$$(ii) \quad [H_1, \mathcal{O}_\pi^-] |\Psi_0\rangle = \mathcal{E} \mathcal{O}_\pi^- |\Psi_0\rangle, \quad (17)$$

$$(iii) \quad [[H_1, \mathcal{O}_\pi^-], \mathcal{O}_\pi^-] |\Psi_0\rangle = 0, \quad (18)$$

$$(iv) \quad [[H_1, \mathcal{O}_\pi^-], \mathcal{O}_\pi^-], \mathcal{O}_\pi^- = 0, \quad (19)$$

where $\mathcal{E} = -2h_y$. The above relations readily imply that the states $|\Psi_n\rangle$ ($n = 0, 1, 2, \dots, L$) are exact eigenstates of $H_1(g, h_y)$ with eigenvalues $(L - 2n)h_y$.

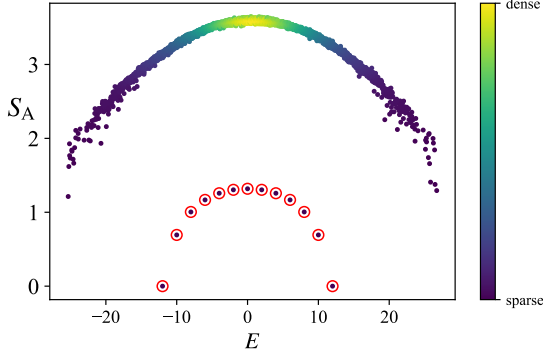


FIG. 2. Half-chain EE S_A as a function of energy E for all eigenstates of $H_1(g=1, h_y=1)$ with $L=12$. The random coefficients c_j are chosen from the interval $[-1, 1]$. The density of data points is color coded. The red solid circles indicate the scar states $|\Psi_n\rangle$ ($n=0, 1, \dots, 12$).

III. MODEL WITHOUT $U(1)$ SYMMETRY AND SCARS

The model constructed in the previous section has a $U(1)$ symmetry corresponding to the spin rotation symmetry about the y axis. In this section, we consider an extension of the model in which this $U(1)$ symmetry is broken explicitly.

Again, our starting point is the tilted Néel states. One can prove that they are IBS of the XYZ model:

$$\begin{aligned} H_{\text{XYZ}} &= \sum_{j=1}^L h_{j,j+1}^{\text{XYZ}} \\ &= \sum_{j=1}^L (J_x \sigma_j^x \sigma_{j+1}^x + J_y \sigma_j^y \sigma_{j+1}^y + J_z \sigma_j^z \sigma_{j+1}^z). \end{aligned} \quad (20)$$

(See Appendix A for a proof.) Thus, it follows that the third conserved charge Q_3 of the XYZ model annihilates $|\psi_{1,2}(\alpha)\rangle$ in Eqs. (9) and (10). Therefore, $|\Psi_n\rangle$ in Eq. (13) are eigenstates of the following Hamiltonian:

$$H_2(g, h_y) = Q_3 + gH_{\text{pert}} + h_y Y, \quad (21)$$

with eigenvalues $(L-2n)h_y$. Using the boost operator B [78, 85–87], one can explicitly construct the third conserved charge of the XYZ model via $Q_3 = i[B, H_{\text{XYZ}}]$ ⁵.

⁵ Alternatively, higher order local conserved quantities can be obtained using the method in [88]

As a result, we obtain [86]

$$\begin{aligned} Q_3 &= \sum_{j=1}^L \hat{\sigma}_j \cdot (\bar{\sigma}_{j+1} \times \hat{\sigma}_{j+2}) \\ &= \sum_{j=1}^L \sum_{\lambda, \mu, \nu} \epsilon_{\lambda\mu\nu} \frac{J_x J_y J_z}{J_\mu} \sigma_j^\lambda \sigma_{j+1}^\mu \sigma_{j+2}^\nu, \end{aligned} \quad (22)$$

where

$$\hat{\sigma}_j^\mu = \sqrt{J_\mu} \sigma_j^\mu, \quad (23)$$

$$\bar{\sigma}_j^\mu = \sqrt{\frac{J_x J_y J_z}{J_\mu}} \sigma_j^\mu, \quad (24)$$

and $\epsilon_{\lambda\mu\nu}$ is the Levi-Civita symbol with $\epsilon_{xyz} = 1$. Clearly, Q_3 reduces to C_{SC} in Eq. (4) when $J_x = J_y = J_z = 1$. It should be noted that the Hamiltonian $H_2(g, h_y)$ breaks $U(1)$ spin rotation symmetry about the y -axis when $J_x \neq J_z$.

To confirm that $|\Psi_n\rangle$ are low-entanglement states in the middle of the spectrum, we compute the half-chain EE for all energy eigenstates of the Hamiltonian (21). Figure 3 shows the numerical results, where the states $|\Psi_n\rangle$ are in the middle of the spectrum and stand out as entanglement outliers with significantly lower entanglement than the other states. This observation leads us to conclude that they are QMBS of the Hamiltonian (21).

We remark that the tower of QMBS in $H_2(g, h_y)$ can also be explained by an RSGA of order 2 when $J_x = J_z$, where $U(1)$ symmetry is manifest. However, when $J_x \neq J_z$, $H_2(g, h_y)$ does not admit this RSGA. Instead, the Hamiltonian exhibits an RSGA of order 4. We have checked this numerically for $L \leq 12$ for various values of the parameters.

IV. DYNAMICS

To reveal the nonthermal features of the scar states, we study their dynamical behavior. Here we consider the quench dynamics of H_2 in Eq. (21). The initial states we consider are the Néel state $|\mathbb{Z}_2\rangle = |\uparrow\downarrow\uparrow\downarrow\cdots\rangle$ and a period-3 state $|\mathbb{Z}_3\rangle = |\uparrow\uparrow\downarrow\uparrow\uparrow\downarrow\cdots\rangle$. Remarkably, the Néel state can be written as a weighted superposition of QMBS exactly:

$$\begin{aligned} |\mathbb{Z}_2\rangle &= |\uparrow\downarrow\uparrow\downarrow\cdots\rangle = |\psi_1(\alpha \rightarrow \infty)\rangle \\ &= (-1)^{L/2} \frac{i^{L/2}}{2^{L/2}} \sum_{n=0}^L \sqrt{\binom{L}{n}} |\Psi_n\rangle, \end{aligned} \quad (25)$$

which would exhibit perfect revivals when evolved by H_2 . On the other hand, the state $|\mathbb{Z}_3\rangle$ is expected to be a thermal state.

In order to confirm this expectation, we calculate the time evolution of the fidelity $\mathcal{F}(t) := |\langle\phi(t=0)|\phi(t)\rangle| = |\langle\phi|e^{-iH_2 t}|\phi\rangle|$. Figure 4 shows the numerical results for

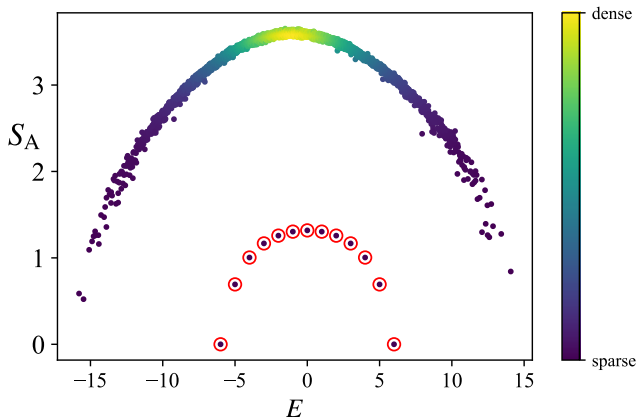


FIG. 3. Half-chain EE S_A as a function of energy E for all eigenstates of $H_2(g = 1.0, h_y = 0.5)$ with $L = 12$ and $(J_x, J_y, J_z) = (0.1, 0.5, 1.0)$. The random coefficients c_j are drawn from the interval $[-1, 1]$. The density of data points is color coded. The red solid circles indicate the half-chain EE and eigenenergy of $|\Psi_n\rangle$ ($n = 0, 1, \dots, 12$).

the fidelity of $|\mathbb{Z}_2\rangle$ and that of $|\mathbb{Z}_3\rangle$. It is clear that the Néel state shows perfectly periodic revivals, which implies that it never reaches thermal equilibrium. We note in passing that a perfect revival of the initial state after a time of at most $\mathcal{O}(\text{poly}(L))$, in general, implies the existence of QMBS [73].

Since $|\mathbb{Z}_2\rangle = |\uparrow\downarrow\uparrow\downarrow\cdots\rangle$ is a zero-energy eigenstate of $H_2(g, h_y = 0)$, we obtain the explicit form of the fidelity of this state:

$$\mathcal{F}(t) = \left| \langle \mathbb{Z}_2 | e^{-itH_2(g, h_y)} | \mathbb{Z}_2 \rangle \right| = \cos^L(h_y t). \quad (26)$$

This readily implies that the fidelity of $|\mathbb{Z}_2\rangle$ shows perfect revivals with period $T = \frac{\pi}{h_y}$, which agrees with the numerical result shown in Figure 4.

To provide further evidence that $|\mathbb{Z}_2\rangle$ is a nonthermal state, we study the time evolution of the spin-spin correlation function:

$$C_r^x(t) = \frac{1}{L} \sum_{j=1}^L \langle \phi(t) | \sigma_j^x \sigma_{j+r}^x | \phi(t) \rangle, \quad (27)$$

where $|\phi(t)\rangle = e^{-itH_2} |\phi\rangle$ with $|\phi\rangle$ being the initial state. Specifically, we consider $|\mathbb{Z}_2\rangle$ and $|\mathbb{Z}_3\rangle$ as initial states. Figure 5 shows the numerical results for $C_r^x(t)$. We can see that $|\mathbb{Z}_2\rangle$ shows perfectly periodic revivals, while $|\mathbb{Z}_3\rangle$ shows no correlation. Since $|\mathbb{Z}_2\rangle$ is a superposition of exact QMBS, the correlation function $C_r^x(t)$ for this state can be calculated analytically. As a result, we obtain

$$C_r^x(t) = (-1)^r \sin^2(2h_y t). \quad (28)$$

From this, we immediately see that $C_r^x(t)$ shows perfect revivals with period $T = \frac{\pi}{2h_y}$. This analytical result agrees with the numerical result shown in Fig. 5.

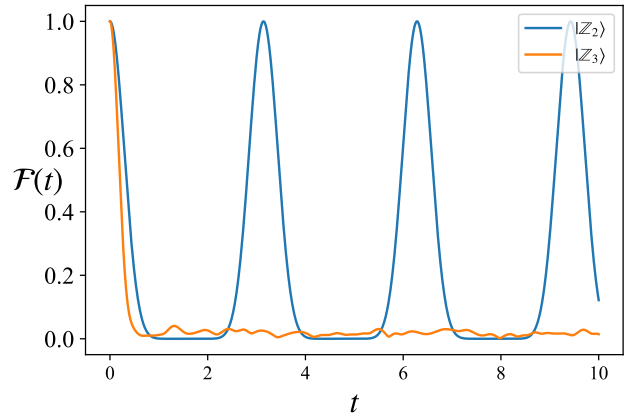


FIG. 4. Fidelity dynamics for the Hamiltonian $H_2(g = 1, h_y = 1)$ [Eq. (21)] with $(J_x, J_y, J_z) = (0.1, 0.5, 1.0)$ and $L = 12$. Each c_j is randomly chosen from $[-1, 1]$. Periodic revivals can be seen when the initial state is $|\mathbb{Z}_2\rangle$ (blue), whereas for $|\mathbb{Z}_3\rangle$ (orange) the fidelity decays rapidly to 0.

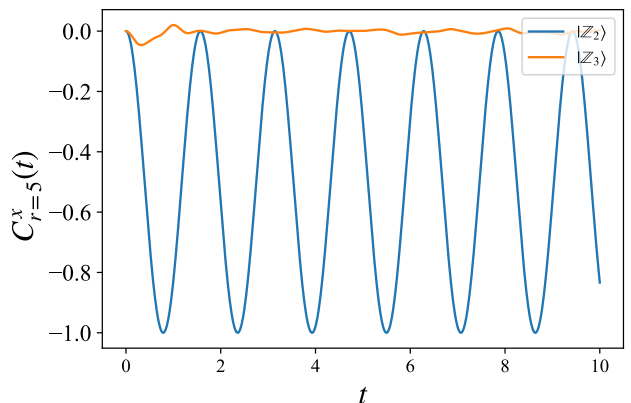


FIG. 5. The time evolution of the correlation function $C_{r=5}^x(t)$ [Eq. (27)] for $|\mathbb{Z}_2\rangle$ (blue) and $|\mathbb{Z}_3\rangle$ (orange). The system size is $L = 12$, and the parameters of Hamiltonian H_2 [Eq. (21)] are $g = 1$, $h_y = 1$ and $(J_x, J_y, J_z) = (0.1, 0.5, 1.0)$. Each c_j is drawn from $[-1, 1]$ randomly.

V. EXTENSION TO HIGHER-DIMENSIONAL LATTICE MODELS

So far, our discussion has been limited to 1D models. One can, however, construct scarred models in higher dimensions in a similar manner. Let us consider a two-dimensional (2D) spin-1/2 model on the $L_x \times L_y$ square lattice Λ with periodic boundary conditions (Fig. 6), where both L_x and L_y are assumed to be even. We denote by σ_j^μ ($\mu = x, y, z$) the Pauli matrices at site $j = (j_x, j_y) \in \Lambda$. The Hamiltonian of the model is given by

$$H^{2d}(g, h_y) = Q_3^{2d} + gH_{\text{pert}}^{2d} + h_y Y^{2d}, \quad (29)$$

where

$$Q_3^{2d} = \sum_{j \in \Lambda} \sum_{a=1}^3 \sum_{b=a+1}^4 \lambda_{e_b - e_a} \hat{\sigma}_{j+e_a} \cdot (\bar{\sigma}_j \times \hat{\sigma}_{j+e_b}), \quad (30)$$

$$H_{\text{pert}}^{2d} = \sum_{\langle i,j \rangle} c_{i,j} (\sigma_i^x \sigma_j^x - \sigma_i^y \sigma_j^y + \sigma_i^z \sigma_j^z + 1), \quad (31)$$

$$Y^{2d} = \sum_{j \in \Lambda} \sigma_j^y, \quad (32)$$

with $(e_1, e_2, e_3, e_4) = (-e_x, -e_y, e_y, e_x)$. See Fig. 6 for the definition of the coordinate system. The interaction in the three-body term Q_3^{2d} takes the form of Eq. (22). The prefactors are chosen to be $(\lambda_{2e_x}, \lambda_{2e_y}, \lambda_{e_x+e_y}, \lambda_{e_x-e_y}) = (\lambda_1, \lambda_2, \lambda_3, \lambda_4)$, which can be arbitrary real numbers. Schematically, we can express Q_3^{2d} using the following diagrams,

$$Q_3^{2d} = \sum_{j \in \Lambda} \left(\lambda_1 \cdot \text{diagram}_1 + \lambda_2 \cdot \text{diagram}_2 + \lambda_3 \cdot \text{diagram}_3 + \lambda_3 \cdot \text{diagram}_4 + \lambda_4 \cdot \text{diagram}_5 + \lambda_4 \cdot \text{diagram}_6 \right), \quad (33)$$

with

$$\text{diagram} := \hat{\sigma}_i \cdot (\bar{\sigma}_j \times \hat{\sigma}_k). \quad (34)$$

We can decompose the 2D Hamiltonian Q_3^{2d} into a collection of 1D Hamiltonians defined on different paths on the 2D square lattice. This can be illustrated as

$$Q_3^{2d} = \lambda_1 \text{diagram}_1 + \lambda_2 \text{diagram}_2 + \lambda_3 \text{diagram}_3 + \lambda_3 \text{diagram}_4 + \lambda_4 \text{diagram}_5 + \lambda_4 \text{diagram}_6, \quad (35)$$

where each red line corresponds to the 1D Hamiltonian (22). The real-valued parameters $\lambda_1, \lambda_2, \lambda_3$, and λ_4 can be chosen to be different. The above decomposition allows us to find the exact QMBS in the 2D model using the same way as in the 1D case. Let us introduce the

following state as a 2D analog of the tilted Néel states:

$$|\psi_1^{2d}(\alpha)\rangle = \frac{1}{\sqrt{\mathcal{N}^{2d}}} \bigotimes_{j \in \Lambda} |\chi_j\rangle, \quad (36)$$

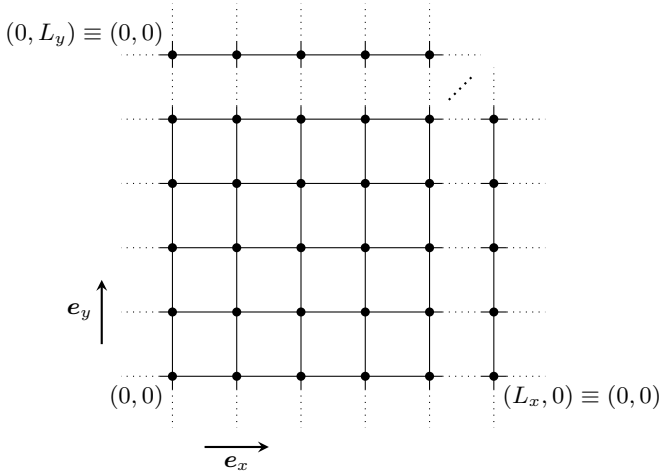


FIG. 6. An example of the $L_x \times L_y$ square lattice, where $\mathbf{e}_x = (1, 0)$ and $\mathbf{e}_y = (0, 1)$. Due to periodic boundary conditions, $(mL_x + x, nL_y + y)$ is identified with (x, y) for any $m, n \in \mathbb{Z}$.

where

$$|\chi_j\rangle = \begin{cases} -\alpha |\uparrow\rangle + |\downarrow\rangle & j_x + j_y \equiv 0 \pmod{2} \\ |\uparrow\rangle + \alpha |\downarrow\rangle & j_x + j_y \equiv 1 \pmod{2} \end{cases}, \quad (37)$$

and the normalization constant is given by $\mathcal{N}^{2d} = (|\alpha|^2 + 1)^N$ with $N = L_x L_y$ denoting the total number of sites in Λ . The other tilted Néel state is obtained as

$$|\psi_2^{2d}(\alpha)\rangle = \mathcal{T}_x |\psi_1^{2d}(\alpha)\rangle = \mathcal{T}_y |\psi_1^{2d}(\alpha)\rangle, \quad (38)$$

where \mathcal{T}_x and \mathcal{T}_y are the translation operators along the x -axis and y -axis, respectively. Each of $|\psi_{1,2}^{2d}(\alpha)\rangle$ can be regarded as an array of 1D tilted Néel states that reside on the red paths in each diagram of Eq. (35). Thus, it is readily seen that these states are zero-energy states of Q_3^{2d} . Similarly to the 1D case, they are annihilated by each local term in H_{pert}^{2d} . Therefore, the 2D tilted Néel states are zero-energy states of $H^{2d}(g, 0) = Q_3^{2d} + gH_{\text{pert}}^{2d}$ for all g .

Similarly to the 1D case, we now consider the projections of $|\psi_1^{2d}(\alpha)\rangle$ onto states with definite magnetization in the y direction. They can be written in terms of the 2D version of the lowering operator as

$$|\Psi_n^{2d}\rangle = \frac{(\mathcal{O}_{2d}^-)^n}{\sqrt{n!N!/(N-n)!}} |+\cdots+\rangle, \quad (39)$$

where

$$\mathcal{O}_{2d}^- = \sum_{j \in \Lambda} (-1)^{(j_x + j_y)} \tilde{\sigma}_j^- \quad (40)$$

with $\tilde{\sigma}_j^- := (\sigma_j^z - i\sigma_j^x)/2$. Following the arguments in Sec. II, we find that $|\Psi_n^{2d}\rangle$ is an eigenstate of the Hamiltonian (29) with eigenvalue $(N - 2n)h_y$.

To confirm that these states are low-entanglement states in the middle of the spectrum, we compute the EE

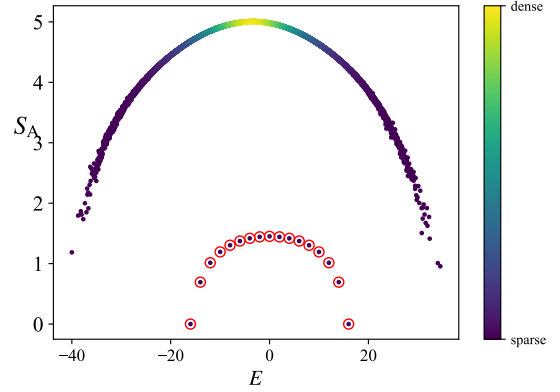


FIG. 7. Half-system EE S_A as a function of energy E for all eigenstates of the Hamiltonian (29) with $(L_x, L_y) = (4, 4)$. The parameters of the Hamiltonian are $g = h_y = 1$ and $(J_x, J_y, J_z) = (0.1, 0.5, 1.0)$. The random coefficients $c_{i,j}$ are chosen from an interval $[-1, 1]$. The density of data points is color coded. The red solid circles indicate $|\Psi_n^{2d}\rangle$.

for all energy eigenstates of the Hamiltonian (29). We divide the lattice Λ into two halves A and B ($\Lambda = A \sqcup B$). Here, $A = \{\mathbf{j} \in \Lambda | j_y < L_y/2\}$ denotes the lower half, while B denotes its complement. The analytical calculation of the half-system EE for QMBS, i.e., $S_A(|\Psi_n^{2d}\rangle)$, proceeds along the same lines as that of the ferromagnetic states discussed in [55]. The result reads

$$S_A(|\Psi_n^{2d}\rangle) = - \sum_{k=0}^{\min(n, N-n)} \frac{\binom{N/2}{k} \binom{N/2}{n-k}}{\binom{N}{n}} \ln \frac{\binom{N/2}{k} \binom{N/2}{n-k}}{\binom{N}{n}}. \quad (41)$$

In particular, at $n = N/2$, it takes the maximum value, which is evaluated as

$$S_A(|\Psi_{n=N/2}^{2d}\rangle) = \frac{1}{2} \ln \frac{e\pi N}{8} + O(N^{-1}). \quad (42)$$

Thus, the entanglement entropy of $|\Psi_n^{2d}\rangle$ obeys the sub-volume law, suggesting that these states are QMBS. Figure 7 shows the numerical results for the half-system EE for all eigenstates of $H^{2d}(g, h_y)$. Clearly, the states $|\Psi_n^{2d}\rangle$ are in the middle of the spectrum and stand out as entanglement outliers with extremely low entanglement. Their half-system EE perfectly match the analytical results (41). These results provide strong evidence that our 2D model is a scarred model with exact QMBS.

Finally, we mention that our result can be expanded for models on any bipartite graph, for example, the honeycomb lattice. Here, a graph $G = (V, E)$ is bipartite if there exists a direct sum decomposition of the set of vertices $V = A \sqcup B$ such that any edge $e \in E$ connects a vertex in A and one in B . For a bipartite graph $G = (V, E)$, we introduce the following Hamiltonian

$$H^G(g, h_y) = Q^G + gH_{\text{pert}}^G + h_y Y^G, \quad (43)$$

with

$$Q^G = \sum_{\langle ij \rangle, \langle jk \rangle \in E} \hat{\sigma}_i \cdot (\hat{\sigma}_j \times \hat{\sigma}_k), \quad (44)$$

$$H_{\text{pert}}^G = \sum_{\langle ij \rangle \in E} c_{\langle ij \rangle} (\sigma_i^x \sigma_j^x - \sigma_i^y \sigma_j^y + \sigma_i^z \sigma_j^z + 1), \quad (45)$$

$$Y^G = \sum_{v \in V} \sigma_v^y. \quad (46)$$

Similarly to the square-lattice case, one can define the lowering operator as

$$\mathcal{O}_G^- = \sum_{v_a \in A} \tilde{\sigma}_{v_a}^- - \sum_{v_b \in B} \tilde{\sigma}_{v_b}^-. \quad (47)$$

By repeatedly acting with this operator on the all-plus state, we can generate a tower of scar states

$$|\Psi_n^G\rangle = (\mathcal{O}_G^-)^n \bigotimes_{v \in V} |+\rangle_v, \quad (48)$$

which are exact eigenstates of $H^G(g, h_y)$. Through the same discussion as in the one-dimensional or 2D square-lattice cases, we can verify that these states violate ETH.

VI. DISCUSSIONS

In this article, we constructed several models with multiple QMBS using IBS. We focused on the tilted-Néel states, which are parametrized IBS of the spin-1/2 Heisenberg and XYZ models, and showed that they serve as parent states of towers of scar states in a class of nonintegrable models. This is in contrast to our previous work, where the models constructed based on IBS exhibit only one or two isolated QMBS that do not admit any non-trivial dynamics such as periodic revivals. Thus, we have significantly improved our previous results, which indicates that the current method using IBS is as useful in constructing QMBS as other existing methods.

Interestingly, the tower of QMBS that we found has an RSGA structure. The existence of an RSGA structure implies that the QMBS generated by this method are equidistant in energy. We remark that, in a different context, a set of ETH-violating states with unequal level spacings has been constructed using the partial solvability [89, 90]. It would be interesting to extend our results in that context too.

For future research, we aim to establish concrete relations between models with QMBS and integrable models. Through the construction of QMBS by our method, we reveal that some models with QMBS are closely related to integrable models through the IBS. Meanwhile, some integrable models possess common algebraic structure, such as Temperley-Lieb algebra [80, 91], chromatic algebra [92, 93], or Birman-Murakami-Wenzl algebra [94, 95]. Additionally, there are integrable models sharing the same algebraic structure but in different algebraic representations. Therefore, it would be worth constructing

different “representations” of QMBS that emerge from IBS in different integrable models of the same algebraic origin. This intuition will provide valuable insights for developing a range of other models featuring QMBS.

ACKNOWLEDGEMENT

The numerical calculations were performed using QuSpin [96, 97]. H. K. is supported by JSPS KAKENHI Grants No. JP23K25783, No. JP23K25790, and MEXT KAKENHI Grant-in-Aid for Transformative Research Areas A “Extreme Universe” (KAKENHI Grant No. JP21H05191). K. S. acknowledges the support of the Forefront Physics and Mathematics Program to Drive Transformation (FoPM). Y. M. would like to thank J. Minař and K. Schoutens for discussions and University of Amsterdam for hospitality. Y.M.’s work is supported by World Premier International Research Center Initiative (WPI), MEXT, Japan.

Appendix A: Proof that the tilted-Néel states are integrable boundary states

In this appendix, we prove that the tilted-Néel states are IBS of the XYZ model. Let us fix $\eta, \tau \in \mathbb{C}$ with $\text{Im}\{\tau\} > 0$, which are the parameters of the elliptic functions in the following. The R -matrix of the XYZ model, acting on $\mathbb{C}_i^2 \otimes \mathbb{C}_j^2$, is given as [91, 98–103]

$$R_{ij}(u) = \begin{pmatrix} a(u) & & & d(u) \\ & b(u) & c(u) & \\ & c(u) & b(u) & \\ d(u) & & & a(u) \end{pmatrix}, \quad (A1)$$

with

$$a(u) = \frac{\theta_4(\eta|2\tau)\theta_1(u+\eta|2\tau)}{\theta_1(\eta|2\tau)\theta_4(u+\eta|2\tau)}, \quad (A2)$$

$$b(u) = \frac{\theta_4(\eta|2\tau)\theta_1(u|2\tau)}{\theta_1(\eta|2\tau)\theta_4(u|2\tau)}, \quad (A3)$$

$$c(u) = 1, \quad (A4)$$

$$d(u) = \frac{\theta_1(u+\eta|2\tau)\theta_1(\eta|2\tau)}{\theta_4(u+\eta|2\tau)\theta_4(\eta|2\tau)}, \quad (A5)$$

where $\theta_n(u|\tau)$ ($n \in \{1, 2, 3, 4\}$) are the four Jacobi theta functions [103, 104] with elliptic nome $q = e^{i\tau}$. This R -matrix satisfies the regularity condition $R_{i,j}(u=0) = P_{i,j}$, where $P_{i,j}$ is a permutation operator such that $P_{i,j}(|x\rangle_i \otimes |y\rangle_j) = |y\rangle_i \otimes |x\rangle_j$. The R -matrix satisfies the following Yang-Baxter equation (Fig. 8):

$$R_{1,2}(u-v)R_{1,3}(u)R_{2,3}(v) = R_{2,3}(v)R_{1,3}(u)R_{1,2}(u-v). \quad (A6)$$

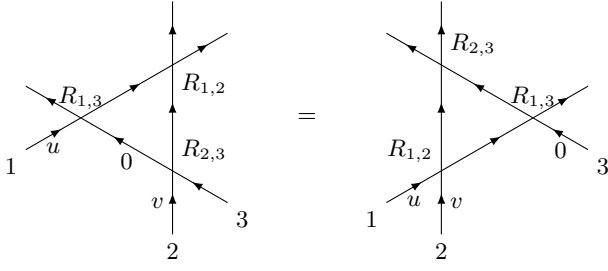


FIG. 8. Graphical representation of the Yang-Baxter equation (Eq. (A6)). We denote $R_{a,b}(u-v) = a \xrightarrow{u} b$. The diagrams are to be read from bottom to top, corresponding to reading (A6) from right to left.

From the R -matrix, we define the transfer matrix $T(u)$:

$$T(u) = \text{Tr}_a \left[\prod_{j=1}^{\overleftarrow{L}} R_{a,j} \left(u - \frac{\eta}{2} \right) \right], \quad (\text{A7})$$

where the multiplication is defined as $\prod_{j=1}^{\overleftarrow{L}} A_j := A_L A_{L-1} \cdots A_1$. Taking the logarithmic derivative of the transfer matrix, we obtain the Hamiltonian and higher-order conserved charges,

$$Q_n = -i \partial_u^{(n-1)} \log T(u)|_{u=0}, \quad (\text{A8})$$

$$H \propto -i \partial_u \log T(u)|_{u=0} \propto Q_2. \quad (\text{A9})$$

Specifically, the anisotropy parameters of the XYZ Hamiltonian (20) are parametrized as

$$J_x = \frac{\theta_4(\eta|\tau)}{\theta_4(0|\tau)}, \quad J_y = \frac{\theta_3(\eta|\tau)}{\theta_3(0|\tau)}, \quad J_z = \frac{\theta_2(\eta|\tau)}{\theta_2(0|\tau)}. \quad (\text{A10})$$

Then we can translate the statement we want to prove into the language of the transfer matrix:

Theorem 1 For $j = 1, 2$ and any $\alpha \in \mathbb{C}$, the following relation holds for tilted Néel states (9) and (10),

$$T(u) |\psi_j(\alpha)\rangle = \mathcal{I} T(u) \mathcal{I} |\psi_j(\alpha)\rangle, \quad j \in \{1, 2\}, \quad (\text{A11})$$

where \mathcal{I} is the parity operator defined as

$$\mathcal{I} = \prod_{j=1}^{L/2} P_{j, L-j+1}. \quad (\text{A12})$$

The proof of this theorem is parallel to the proof that the tilted Néel states are IBS of the XXZ model [56]. As outlined in [56], the IBS can be viewed as integrable boundaries of the partition function of a vertex model, by rotating the products of transfer matrices by $\pi/2$. Therefore, we introduce the boundary Yang-Baxter equation (BYBE) [56, 105–108] (Fig. 9),

$$\begin{aligned} R_{1,2}(u-v) K_{R,1}(u) R_{2,1}(u+v) K_{R,2}(v) \\ = K_{R,2}(v) R_{2,1}(u+v) K_{R,1}(u) R_{1,2}(u-v), \end{aligned} \quad (\text{A13})$$

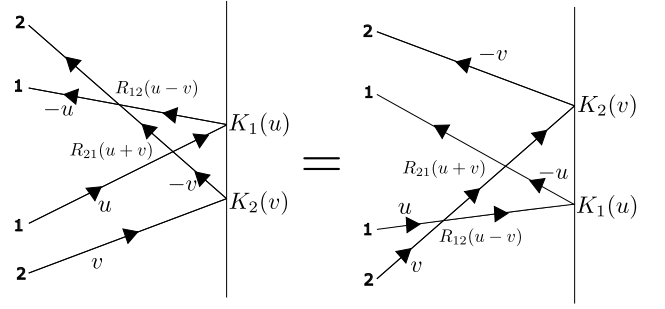


FIG. 9. Graphical representation of the boundary Yang-Baxter equation (Eq. (A13)). The diagrams are to be read from bottom to top, corresponding to reading (A13) from right to left. Note that the signs of the rapidities u and v change at the boundary because of the reflection.

$$\begin{aligned} R_{1,2}(-u+v) K_{L,1}^t(u) R_{2,1}(-u-v-2\eta) K_{L,2}^t(v) \\ = K_{L,2}^t(v) R_{2,1}(-u-v-2\eta) K_{L,1}^t(u) R_{1,2}^t(-u+v), \end{aligned} \quad (\text{A14})$$

where the superscript t denotes the transposition. The matrix $K_{R(L)}$ corresponds to the right (left) boundary condition [56]. We focus on the K matrices with non-vanishing off-diagonal elements, and we find solutions to the BYBE [107],

$$K_{R,a}(u; \xi, \mu, \lambda) = \begin{pmatrix} K^{11}(u) & K^{12}(u) \\ K^{21}(u) & K^{22}(u) \end{pmatrix}_a, \quad (\text{A15})$$

$$K_{L,a}(u) = K_{R,a}^t(-u-\eta), \quad (\text{A16})$$

where $\xi, \mu, \lambda \in \mathbb{C}$ is a free parameter. The matrix elements of the K matrix are

$$K^{11}(u) = \frac{\theta_1(\xi+u|2\tau)}{\theta_4(\xi+u|2\tau)}, \quad K^{22}(u) = \frac{\theta_1(\xi-u|2\tau)}{\theta_4(\xi-u|2\tau)}, \quad (\text{A17})$$

$$K^{12}(u) = \mu \frac{\theta_1(2u|2\tau)}{\theta_4(2u|2\tau)} \frac{\theta_4(\xi|2\tau)^2 (\lambda \epsilon_- + \epsilon_+)}{\epsilon_0}, \quad (\text{A18})$$

$$K^{21}(u) = \mu \frac{\theta_1(2u|2\tau)}{\theta_4(2u|2\tau)} \frac{\theta_4(\xi|2\tau)^2 (\lambda \epsilon_- - \epsilon_+)}{\epsilon_0}, \quad (\text{A19})$$

where the parameters are

$$\epsilon_0 = \theta_4(\xi|2\tau)^2 \theta_4(u|2\tau)^2 - \theta_1(\xi|2\tau)^2 \theta_1(u|2\tau)^2, \quad (\text{A20})$$

$$\epsilon_{\pm} = \theta_4(u|2\tau)^2 \pm \theta_1(u|2\tau)^2. \quad (\text{A21})$$

By considering the $\pi/2$ rotation on the Euclidean spacetime, we obtain the reflection equation [56], as shown in Fig. 10,

$$\begin{aligned} \tilde{R}_{3,4}(-u+v) \tilde{R}_{2,3}(-u-v) \left| \phi_0(u - \frac{\eta}{2}) \right\rangle_{1,2} \left| \phi_0(v - \frac{\eta}{2}) \right\rangle_{3,4} \\ = \tilde{R}_{1,2}(-u+v) \tilde{R}_{2,3}(-u-v) \left| \phi_0(v - \frac{\eta}{2}) \right\rangle_{1,2} \left| \phi_0(u - \frac{\eta}{2}) \right\rangle_{3,4}, \end{aligned} \quad (\text{A22})$$

where $\tilde{R}_{a,b} = R_{a,b} P_{a,b}$ and the boundary state is in the following form [56],

$$\begin{aligned} |\phi_0(u)\rangle = & -K^{12}(u) |\uparrow\uparrow\rangle + K^{11}(u) |\uparrow\downarrow\rangle \\ & -K^{22}(u) |\downarrow\uparrow\rangle + K^{21}(u) |\downarrow\downarrow\rangle. \end{aligned} \quad (\text{A23})$$

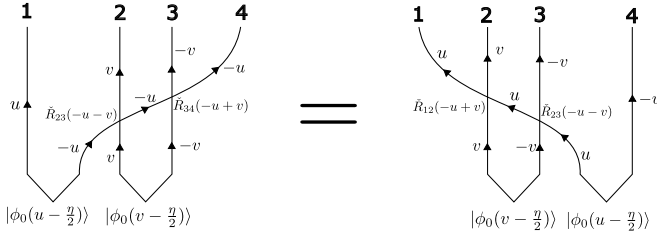


FIG. 10. Graphical representation of the reflection equation (Eq. (A22)). The diagrams are to be read from bottom to top, corresponding to reading (A22) from right to left.

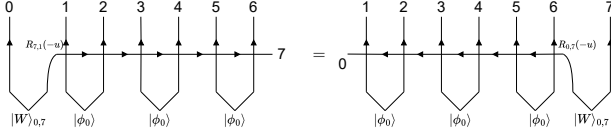


FIG. 11. An illustration of Eq. (A24) with $L = 6$.

We consider a boundary state with $(L+2)$ sites (labeled by $0, 1, \dots, L, (L+1)$) $|\phi_0(u - \frac{\eta}{2})\rangle_{0,1} \otimes |\phi_0(v - \frac{\eta}{2})\rangle_{2,3} \otimes \dots \otimes |\phi_0(v - \frac{\eta}{2})\rangle_{L,L+1}$, as a generalization of the boundary states in Fig. 10. Analogous to (A22), and taking the limit $v \rightarrow 0$, we obtain

$$\begin{aligned} & \prod_{j=1}^L \overleftarrow{R}_{L+1,j}(-u) \left(|W\rangle_{0,L+1} \otimes |\phi_0\rangle^{\otimes \frac{L}{2}} \right) \\ &= \prod_{j=1}^L \overleftarrow{R}_{0,L+1-j}(-u) \left(|\phi_0\rangle^{\otimes \frac{L}{2}} \otimes |W\rangle_{0,L+1} \right), \end{aligned} \quad (\text{A24})$$

where $|\phi_0\rangle = |\phi_0(-\frac{\eta}{2})\rangle$ and $|W\rangle_{0,L+1} = |\phi_0(u - \frac{\eta}{2})\rangle_{0,L+1}$. Eq. (A24) is illustrated in Fig. 11. The sites 0 and $L+1$ are auxiliary sites corresponding to the left and right boundary, respectively.

Finally, by comparing the components of (A24) [56],

we obtain

$$\begin{aligned} & \text{Tr}_{L+1} \left[\prod_{j=1}^L \overleftarrow{R}_{L+1,j}(-u) \right] |\phi_0\rangle^{\otimes \frac{L}{2}} \\ &= \text{Tr}_0 \left[\prod_{j=1}^L \overleftarrow{R}_{0,L+1-j}(-u) \right] |\phi_0\rangle^{\otimes \frac{L}{2}}. \end{aligned} \quad (\text{A25})$$

From the definition of the transfer matrix (A7), the equation above implies

$$T(u) |\phi_0\rangle^{\otimes \frac{L}{2}} = \mathcal{I} T(u) \mathcal{I} |\phi_0\rangle^{\otimes \frac{L}{2}}, \quad (\text{A26})$$

satisfying the IBS condition.

Taking the limit $\lambda \rightarrow \infty$ with $\lim_{\lambda \rightarrow \infty} \mu\lambda = \zeta \in O(1)$ in (A23), and defining $\alpha = \sqrt{\frac{K^{11}(-\eta/2)}{K^{22}(-\eta/2)}}$, the boundary state reads

$$\begin{aligned} |\phi_0\rangle^{\otimes \frac{L}{2}} &\propto \left(-\alpha^2 |\uparrow\downarrow\rangle + |\downarrow\uparrow\rangle + \right. \\ &\quad \left. \zeta w (-|\uparrow\uparrow\rangle + |\downarrow\downarrow\rangle) \right)^{\otimes \frac{L}{2}}, \end{aligned} \quad (\text{A27})$$

where the constant is

$$w = \frac{\theta_1(-\eta|2\tau)\theta_4(\xi|2\tau)^2}{\theta_4(-\eta|2\tau)} \frac{\epsilon_-}{\epsilon_0} \Big|_{u=-\frac{\eta}{2}}. \quad (\text{A28})$$

If we further require that $\zeta = \frac{\alpha}{w}$, we obtain

$$\begin{aligned} |\phi_0\rangle^{\otimes \frac{L}{2}} &\propto \left[-\alpha^2 |\uparrow\downarrow\rangle + |\downarrow\uparrow\rangle \right. \\ &\quad \left. + \alpha (-|\uparrow\uparrow\rangle + |\downarrow\downarrow\rangle) \right]^{\otimes \frac{L}{2}} \\ &\propto |\psi_1(\alpha)\rangle, \end{aligned} \quad (\text{A29})$$

i.e. the tilted Néel state. Similar results can be obtained for $|\psi_2(\alpha)\rangle = \prod_{n=1}^{L-1} P_{n,n+1} |\psi_1(\alpha)\rangle$. Therefore, the tilted Néel states are also IBS of the XYZ model, proving Theorem 1.

- [1] J. von Neumann, Beweis des Ergodensatzes und des H-Theorems in der neuen Mechanik, *Z. Phys.* **57**, 30 (1929).
- [2] H. Ekstein, Ergodic Theorem for Interacting Systems, *Phys. Rev.* **107**, 333 (1957).
- [3] M. V. Berry, Regular and irregular semiclassical wavefunctions, *J. Phys. A: Math. Gen.* **10**, 2083 (1977).
- [4] J. M. Deutsch, Quantum statistical mechanics in a closed system, *Phys. Rev. A* **43**, 2046 (1991).
- [5] M. Srednicki, Chaos and quantum thermalization, *Phys. Rev. E* **50**, 888 (1994).
- [6] J. M. Deutsch, Eigenstate thermalization hypothesis, *Rep. Prog. Phys.* **81**, 082001 (2018).
- [7] M. Rigol, V. Dunjko, and M. Olshanii, Thermalization

and its mechanism for generic isolated quantum systems, *Nature (London)* **452**, 854 (2008).

- [8] A. Polkovnikov, K. Sengupta, A. Silva, and M. Vengalattore, Colloquium: Nonequilibrium dynamics of closed interacting quantum systems, *Rev. Mod. Phys.* **83**, 863 (2011).
- [9] R. Nandkishore and D. A. Huse, Many-body localization and thermalization in quantum statistical mechanics, *Annu. Rev. Condens. Matter Phys.* **6**, 15 (2015).
- [10] L. D'Alessio, Y. Kafri, A. Polkovnikov, and M. Rigol, From quantum chaos and eigenstate thermalization to statistical mechanics and thermodynamics, *Adv. Phys.* **65**, 239 (2016).
- [11] M. Brenes, T. LeBlond, J. Goold, and M. Rigol, Eigen-

- state Thermalization in a Locally Perturbed Integrable System, *Phys. Rev. Lett.* **125**, 070605 (2020).
- [12] M. Brenes, J. Goold, and M. Rigol, Low-frequency behavior of off-diagonal matrix elements in the integrable XXZ chain and in a locally perturbed quantum-chaotic XXZ chain, *Phys. Rev. B* **102**, 075127 (2020).
- [13] D. A. Abanin and Z. Papić, Recent progress in many-body localization, *Ann. Phys. (Berlin)* **529**, 1700169 (2017).
- [14] D. A. Abanin, E. Altman, I. Bloch, and M. Serbyn, Colloquium: Many-body localization, thermalization, and entanglement, *Rev. Mod. Phys.* **91**, 021001 (2019).
- [15] F. Alet and N. Laflorencie, Many-body localization: An introduction and selected topics, *C. R. Phys.* **19**, 498 (2018).
- [16] S. Moudgalya, B. A. Bernevig, and N. Regnault, Quantum many-body scars and Hilbert space fragmentation: a review of exact results, *Rep. Prog. Phys.* **85**, 086501 (2022).
- [17] S. Moudgalya and O. I. Motrunich, Hilbert Space Fragmentation and Commutant Algebras, *Phys. Rev. X* **12**, 011050 (2022).
- [18] P. Brighi, M. Ljubotina, and M. Serbyn, Hilbert space fragmentation and slow dynamics in particle-conserving quantum East models, *SciPost Phys.* **15**, 093 (2023).
- [19] C. Neill, P. Roushan, M. Fang, Y. Chen, M. Kolodrubetz, Z. Chen, A. Megrant, R. Barends, B. Campbell, B. Chiaro, A. Dunsworth, E. Jeffrey, J. Kelly, J. Mutus, P. J. J. O'Malley, C. Quintana, D. Sank, A. Vainsencher, J. Wenner, T. C. White, A. Polkovnikov, and J. M. Martinis, Ergodic dynamics and thermalization in an isolated quantum system, *Nat. Phys.* **12**, 1037 (2016).
- [20] A. Morvan, T. I. Andersen, X. Mi, C. Neill, *et al.*, Formation of robust bound states of interacting microwave photons, *Nature (London)* **612**, 240 (2022).
- [21] J. Smith, A. Lee, P. Richerme, B. Neyenhuis, P. W. Hess, P. Hauke, M. Heyl, D. A. Huse, and C. Monroe, Many-body localization in a quantum simulator with programmable random disorder, *Nat. Phys.* **12**, 907 (2016).
- [22] S. Trotzky, Y.-A. Chen, A. Flesch, I. P. McCulloch, U. Schollwöck, J. Eisert, and I. Bloch, Probing the relaxation towards equilibrium in an isolated strongly correlated one-dimensional Bose gas, *Nat. Phys.* **8**, 325 (2012).
- [23] T. Langen, R. Geiger, and J. Schmiedmayer, Ultracold Atoms Out of Equilibrium, *Annu. Rev. Condens. Matter Phys.* **6**, 201 (2015).
- [24] M. Ueda, Quantum equilibration, thermalization and prethermalization in ultracold atoms, *Nat. Rev. Phys.* **2**, 669 (2020).
- [25] H. Bernien, S. Schwartz, A. Keesling, H. Levine, A. Omran, H. Pichler, S. Choi, A. S. Zibrov, M. Endres, M. Greiner, V. Vuletić, and M. D. Lukin, Probing many-body dynamics on a 51-atom quantum simulator, *Nature (London)* **551**, 579 (2017).
- [26] C. S. Adams, J. D. Pritchard, and J. P. Shaffer, Rydberg atom quantum technologies, *J. Phys. B: At. Mol. Opt. Phys.* **53**, 012002 (2019).
- [27] E. J. Heller, Bound-State Eigenfunctions of Classically Chaotic Hamiltonian Systems: Scars of Periodic Orbits, *Phys. Rev. Lett.* **53**, 1515 (1984).
- [28] L. Kaplan and E. Heller, Linear and Nonlinear Theory of Eigenfunction Scars, *Ann. Phys. (N. Y.)* **264**, 171–206 (1998).
- [29] C. J. Turner, A. A. Michailidis, D. A. Abanin, M. Serbyn, and Z. Papić, Weak ergodicity breaking from quantum many-body scars, *Nat. Phys.* **14**, 745 (2018).
- [30] M. Serbyn, D. A. Abanin, and Z. Papić, Quantum many-body scars and weak breaking of ergodicity, *Nat. Phys.* **17**, 675 (2021).
- [31] G.-X. Su, H. Sun, A. Hudomal, J.-Y. Desaulles, Z.-Y. Zhou, B. Yang, J. C. Halimeh, Z.-S. Yuan, Z. Papić, and J.-W. Pan, Observation of many-body scarring in a Bose-Hubbard quantum simulator, *Phys. Rev. Res.* **5**, 023010 (2023).
- [32] P. Zhang, H. Dong, Y. Gao, L. Zhao, J. Hao, J.-Y. Desaulles, Q. Guo, J. Chen, J. Deng, B. Liu, W. Ren, Y. Yao, X. Zhang, S. Xu, K. Wang, F. Jin, X. Zhu, B. Zhang, H. Li, C. Song, Z. Wang, F. Liu, Z. Papić, L. Ying, H. Wang, and Y.-C. Lai, Many-body Hilbert space scarring on a superconducting processor, *Nat. Phys.* **19**, 120 (2023).
- [33] J. Austin-Harris, I. Rana, S. Begg, C. Binegar, T. Bilitewski, and Y. Liu, Observation of ergodicity breaking and quantum many-body scars in spinor gases (2024), [arXiv:2410.09015 \[cond-mat.quant-gas\]](https://arxiv.org/abs/2410.09015).
- [34] C. J. Turner, A. A. Michailidis, D. A. Abanin, M. Serbyn, and Z. Papić, Quantum scarred eigenstates in a Rydberg atom chain: Entanglement, breakdown of thermalization, and stability to perturbations, *Phys. Rev. B* **98**, 155134 (2018).
- [35] M. Schecter and T. Iadecola, Weak Ergodicity Breaking and Quantum Many-Body Scars in Spin-1 XY Magnets, *Phys. Rev. Lett.* **123**, 147201 (2019).
- [36] S. Choi, C. J. Turner, H. Pichler, W. W. Ho, A. A. Michailidis, Z. Papić, M. Serbyn, M. D. Lukin, and D. A. Abanin, Emergent SU(2) dynamics and perfect quantum many-body scars, *Phys. Rev. Lett.* **122**, 220603 (2019).
- [37] C.-J. Lin and O. I. Motrunich, Exact quantum many-body scar states in the Rydberg-blockaded atom chain, *Phys. Rev. Lett.* **122**, 173401 (2019).
- [38] T. Iadecola and M. Schecter, Quantum many-body scar states with emergent kinetic constraints and finite-entanglement revivals, *Phys. Rev. B* **101**, 024306 (2020).
- [39] C. M. Langlett and S. Xu, Hilbert space fragmentation and exact scars of generalized Fredkin spin chains, *Phys. Rev. B* **103**, L220304 (2021).
- [40] Z. Papić, Weak Ergodicity Breaking Through the Lens of Quantum Entanglement, in *Entanglement in Spin Chains: From Theory to Quantum Technology Applications*, edited by A. Bayat, S. Bose, and H. Johanneson (Springer International Publishing, Cham, 2022) pp. 341–395.
- [41] A. Chandran, T. Iadecola, V. Khemani, and R. Moessner, Quantum Many-Body Scars: A Quasiparticle Perspective, *Annu. Rev. Condens. Matter Phys.* **14**, 443 (2023).
- [42] K. Pakrouski, P. N. Pallegar, F. K. Popov, and I. R. Klebanov, Many-Body Scars as a Group Invariant Sector of Hilbert Space, *Phys. Rev. Lett.* **125**, 230602 (2020).
- [43] K. Pakrouski, P. N. Pallegar, F. K. Popov, and I. R. Klebanov, Group theoretic approach to many-body scar states in fermionic lattice models, *Phys. Rev. Res.* **3**, 043156 (2021).
- [44] Z. Sun, F. K. Popov, I. R. Klebanov, and K. Pakrouski,

- Majorana scars as group singlets, *Phys. Rev. Res.* **5**, 043208 (2023).
- [45] M. Kunimi, T. Tomita, H. Katsura, and Y. Kato, Proposal for simulating quantum spin models with the Dzyaloshinskii-Moriya interaction using Rydberg atoms and the construction of asymptotic quantum many-body scar states, *Phys. Rev. A* **110**, 043312 (2024).
- [46] N. Shiraishi and T. Mori, Systematic Construction of Counterexamples to the Eigenstate Thermalization Hypothesis, *Phys. Rev. Lett.* **119**, 030601 (2017).
- [47] N. O’Dea, F. Burnell, A. Chandran, and V. Khemani, From tunnels to towers: Quantum scars from Lie algebras and q -deformed Lie algebras, *Phys. Rev. Res.* **2**, 043305 (2020).
- [48] N. Shibata, N. Yoshioka, and H. Katsura, Onsager’s Scars in Disordered Spin Chains, *Phys. Rev. Lett.* **124**, 180604 (2020).
- [49] S. Moudgalya, E. O’Brien, B. A. Bernevig, P. Fendley, and N. Regnault, Large classes of quantum scarred Hamiltonians from matrix product states, *Phys. Rev. B* **102**, 085120 (2020).
- [50] D. K. Mark and O. I. Motrunich, η -pairing states as true scars in an extended Hubbard model, *Phys. Rev. B* **102**, 075132 (2020).
- [51] P. A. McClarty, M. Haque, A. Sen, and J. Richter, Disorder-free localization and many-body quantum scars from magnetic frustration, *Phys. Rev. B* **102**, 224303 (2020).
- [52] J. Ren, C. Liang, and C. Fang, Quasisymmetry groups and many-body scar dynamics, *Phys. Rev. Lett.* **126**, 120604 (2021).
- [53] J. Ren, C. Liang, and C. Fang, Deformed symmetry structures and quantum many-body scar subspaces, *Phys. Rev. Res.* **4**, 013155 (2022).
- [54] K. Omiya and M. Müller, Fractionalization paves the way to local projector embeddings of quantum many-body scars, *Phys. Rev. B* **108**, 054412 (2023).
- [55] K. Sanada, Y. Miao, and H. Katsura, Quantum many-body scars in spin models with multibody interactions, *Phys. Rev. B* **108**, 155102 (2023).
- [56] L. Piroli, B. Pozsgay, and E. Vernier, What is an integrable quench?, *Nucl. Phys. B* **925**, 362 (2017).
- [57] M. De Leeuw, C. Kristjansen, and G. Linardopoulos, Scalar one-point functions and matrix product states of AdS/dCFT, *Phys. Lett. B* **781**, 238 (2018).
- [58] B. Pozsgay, Overlaps with arbitrary two-site states in the XXZ spin chain, *J. Stat. Mech.: Theory Exp.* **2018** (5), 053103.
- [59] L. Piroli, E. Vernier, P. Calabrese, and B. Pozsgay, Integrable quenches in nested spin chains I: the exact steady states, *J. Stat. Mech.: Theory Exp.* **2019** (6), 063103.
- [60] B. Pozsgay, L. Piroli, and E. Vernier, Integrable matrix product states from boundary integrability, *SciPost Phys.* **6**, 062 (2019).
- [61] B. Wouters, J. De Nardis, M. Brockmann, D. Fioretto, M. Rigol, and J.-S. Caux, Quenching the Anisotropic Heisenberg Chain: Exact Solution and Generalized Gibbs Ensemble Predictions, *Phys. Rev. Lett.* **113**, 117202 (2014).
- [62] B. Pozsgay, M. Mestyán, M. A. Werner, M. Kormos, G. Zaránd, and G. Takács, Correlations after Quantum Quenches in the XXZ Spin Chain: Failure of the Generalized Gibbs Ensemble, *Phys. Rev. Lett.* **113**, 117203 (2014).
- [63] J.-S. Caux, The Quench Action, *J. Stat. Mech.: Theory Exp.* **2016** (6), 064006.
- [64] M. de Leeuw, C. Kristjansen, and K. Zarembo, One-point Functions in Defect CFT and Integrability, *J. High Energy Phys.* **2015** (08), 098.
- [65] I. Buhl-Mortensen, M. de Leeuw, C. Kristjansen, and K. Zarembo, One-point Functions in AdS/dCFT from Matrix Product States, *J. High Energy Phys.* **2016** (02), 052.
- [66] O. Foda and K. Zarembo, Overlaps of partial Néel states and Bethe states, *J. Stat. Mech.: Theory Exp.* **2016** (2), 023107.
- [67] J. Caetano and S. Komatsu, Crosscap States in Integrable Field Theories and Spin Chains, *J. Stat. Phys.* **187**, 30 (2022).
- [68] T. Gombor, Integrable crosscap states in $\mathfrak{gl}(N)$ spin chains, *J. High Energy Phys.* **2022** (10), 096.
- [69] C. Ekman, Crosscap states in the XXX spin-1/2 spin chain (2022), [arXiv:2207.12354 \[hep-th\]](https://arxiv.org/abs/2207.12354).
- [70] M. He and Y. Jiang, Integrable crosscap states: from spin chains to 1D Bose gas, *J. High Energy Phys.* **2023** (08), 079.
- [71] Y. Chiba and Y. Yoneta, Exact thermal eigenstates of nonintegrable spin chains at infinite temperature, *Phys. Rev. Lett.* **133**, 170404 (2024).
- [72] X.-L. Qi and D. Ranard, Determining a local Hamiltonian from a single eigenstate, *Quantum* **3**, 159 (2019).
- [73] A. M. Alhambra, A. Anshu, and H. Wilming, Revivals imply quantum many-body scars, *Phys. Rev. B* **101**, 205107 (2020).
- [74] O. Bohigas, M. J. Giannoni, and C. Schmit, Characterization of Chaotic Quantum Spectra and Universality of Level Fluctuation Laws, *Phys. Rev. Lett.* **52**, 1 (1984).
- [75] D. Kundu, S. Kumar, and S. Sen Gupta, Signatures of spectral crossovers in the short- and long-range spectral correlations of a disordered spin-chain with Kramers degeneracy, *Phys. Rev. B* **107**, 094205 (2023).
- [76] W. Buijsman, V. Cheianov, and V. Gritsev, Random Matrix Ensemble for the Level Statistics of Many-Body Localization, *Phys. Rev. Lett.* **122**, 180601 (2019).
- [77] L. Piroli, B. Pozsgay, and E. Vernier, From the quantum transfer matrix to the quench action: the Loschmidt echo in XXZ Heisenberg spin chains, *J. Stat. Mech.: Theory Exp.* **2017** (2), 023106.
- [78] M. P. Grabowski and P. Mathieu, Quantum Integrals of Motion for the Heisenberg Spin Chain, *Mod. Phys. Lett. A* **09**, 2197 (1994).
- [79] H. Frahm and C. Rödenbeck, Properties of the chiral spin liquid state in generalized spin ladders, *J. Phys. A: Math. Gen.* **30**, 4467 (1997).
- [80] H. N. V. Temperley, E. H. Lieb, and S. F. Edwards, Relations between the ‘percolation’ and ‘colouring’ problem and other graph-theoretical problems associated with regular planar lattices: some exact results for the ‘percolation’ problem, *Proc. R. Soc. A* **322**, 251 (1971).
- [81] V. Pasquier and H. Saleur, Common structures between finite systems and conformal field theories through quantum groups, *Nucl. Phys. B* **330**, 523 (1990).
- [82] V. Popkov and M. Salerno, Logarithmic divergence of the block entanglement entropy for the ferromagnetic Heisenberg model, *Phys. Rev. A* **71**, 012301 (2005).
- [83] D. K. Mark, C.-J. Lin, and O. I. Motrunich, Unified structure for exact towers of scar states in the Affleck-Kennedy-Lieb-Tasaki and other models, *Phys. Rev. B*

- 101**, 195131 (2020).
- [84] S. Moudgalya, N. Regnault, and B. A. Bernevig, η -pairing in Hubbard models: From spectrum generating algebras to quantum many-body scars, *Phys. Rev. B* **102**, 085140 (2020).
 - [85] E. K. Sklyanin, Quantum inverse scattering method. selected topics (1992), [arXiv:hep-th/9211111 \[hep-th\]](#).
 - [86] M. Grabowski and P. Mathieu, Structure of the conservation laws in quantum integrable spin chains with short range interactions, *Ann. Phys. (N. Y.)* **243**, 299 (1995).
 - [87] M. De Leeuw, A. Pribytok, and P. Ryan, Classifying integrable spin-1/2 chains with nearest neighbour interactions, *J. Phys. A: Math. Theor.* **52**, 505201 (2019).
 - [88] Y. Nozawa and K. Fukai, Explicit construction of local conserved quantities in the XYZ spin-1/2 chain, *Phys. Rev. Lett.* **125**, 090602 (2020).
 - [89] C. Matsui, Exactly solvable subspaces of nonintegrable spin chains with boundaries and quasiparticle interactions, *Phys. Rev. B* **109**, 104307 (2024).
 - [90] C. Matsui and N. Tsuji, Boundary dissipative spin chains with partial solvability inherited from system Hamiltonians (2024), [arXiv:2409.03208 \[cond-mat.stat-mech\]](#).
 - [91] R. J. Baxter, *Exactly solved models in statistical mechanics* (Elsevier, Amsterdam, 2016).
 - [92] P. Fendley and V. Krushkal, Link invariants, the chromatic polynomial and the Potts model, *Adv. Theor. Math. Phys.* **14**, 507 (2010).
 - [93] L. Eck and P. Fendley, From the XXZ chain to the integrable Rydberg-blockade ladder via non-invertible duality defects, *SciPost Physics* **16**, 127 (2024).
 - [94] P. P. Kulish, N. Manojlović, and Z. Nagy, Symmetries of spin systems and Birman–Wenzl–Murakami algebra, *J. Math. Phys.* **51**, 043516 (2010).
 - [95] V. Belavin and D. Gepner, On the algebraic approach to solvable lattice models, *J. High Energy Phys.* **2019** (2), 33.
 - [96] P. Weinberg and M. Bukov, QuSpin: a Python package for dynamics and exact diagonalisation of quantum many body systems part I: spin chains, *SciPost Phys.* **2**, 003 (2017).
 - [97] P. Weinberg and M. Bukov, QuSpin: a Python package for dynamics and exact diagonalisation of quantum many body systems. Part II: bosons, fermions and higher spins, *SciPost Phys.* **7**, 020 (2019).
 - [98] R. J. Baxter, Eight-Vertex Model in Lattice Statistics, *Phys. Rev. Lett.* **26**, 832 (1971).
 - [99] R. Baxter, Eight-vertex model in lattice statistics and one-dimensional anisotropic heisenberg chain. I. Some fundamental eigenvectors, *Ann. Phys. (N. Y.)* **76**, 1 (1973).
 - [100] R. Baxter, Eight-vertex model in lattice statistics and one-dimensional anisotropic heisenberg chain. II. Equivalence to a generalized ice-type lattice model, *Ann. Phys. (N. Y.)* **76**, 25 (1973).
 - [101] R. Baxter, Eight-vertex model in lattice statistics and one-dimensional anisotropic heisenberg chain. III. Eigenvectors of the transfer matrix and hamiltonian, *Ann. Phys. (N. Y.)* **76**, 48 (1973).
 - [102] J. Cao, S. Cui, W.-L. Yang, K. Shi, and Y. Wang, Spin-1/2 XYZ model revisit: General solutions via off-diagonal Bethe ansatz, *Nucl. Phys. B* **886**, 185 (2014).
 - [103] N. Slavnov, A. Zabrodin, and A. Zotov, Scalar products of Bethe vectors in the 8-vertex model, *J. High Energy Phys.* **2020** (06), 123.
 - [104] I. S. Gradshteyn and I. M. Ryzhik, *Table of integrals, series, and products* (Academic press, Cambridge, 2014).
 - [105] E. K. Sklyanin, Boundary conditions for integrable quantum systems, *J. Phys. A: Math. Gen.* **21**, 2375 (1988).
 - [106] H. J. de Vega and A. González-Ruiz, Boundary K-matrices for the XYZ, XXZ and XXX spin chains, *J. Phys. A: Math. Gen.* **27**, 6129 (1994).
 - [107] T. Inami and H. Konno, Integrable XYZ spin chain with boundaries, *J. Phys. A: Math. Gen.* **27**, L913 (1994).
 - [108] T. Kimura and R.-D. Zhu, Bethe/gauge correspondence for SO/Sp gauge theories and open spin chains, *J. High Energy Phys.* **2021** (3), 227.